Indian Journal of Chemistry
Vol. 63, October 2024, pp. 1015-1027
DOI: 10.56042/ijc.v63i10.12704

Synthesis, characterization, thermal aspects, density functional theory study and *in vitro* antibacterial evaluation of Cr(III) complexes based on pyrazolone phenylhydrazone ligands

Chintan P Somaiya*[a], Dinesh S Patel[b], Darshan H Jani[c] & Drashti R Thanki[a]

[a] Department of Chemical Science, Parul Institute of Applied Sciences, Parul University, Vadodara 391 760, Gujarat, India

[b] Shree P. M. Patel Institute of Post Graduate Studies and Research in Science
(Recognized Research Center of Sardar Patel University, V.V. Nagar) Anand 388 001, Gujarat, India

[c] Department of Chemistry, Faculty of Science, Noble University, Bhesan Road Bamangam, Junagadh 362 310, Gujarat, India

E- mail: somaiyachintan11@gmail.com

Received 23 July 2024; accepted(revised) 20 September 2024

This study examines the synthesis, characterization, computational analysis, and antibacterial activity of chromium (III) complexes with pyrazolone phenylhydrazone ligands. The ligands and their chromium (III) complexes have been synthesized and confirmed using various analytical techniques such as ^{1}H and ^{13}C NMR, mass spectrometry, elemental analysis, infrared spectroscopy, and UV-visible spectroscopy. The characterization of chromium (III) complexes involves elemental analysis, thermogravimetric analysis (TGA/DTG), differential scanning calorimetry (DSC), FAB mass spectrometry, and UV-visible spectroscopy, which validated their structures and properties. Additionally, the electronic properties and reactivity of the ligands and complexes have been investigated using DFT with the B3LYP/6-31G(d, p) basis set. The antimicrobial efficacy of the ligands and complexes have been tested against Gram-positive and Gram-negative bacteria, revealing significant antibacterial potential. These findings highlight the importance of pyrazolone phenylhydrazone-based chromium (III) complexes and suggest further exploration of their antimicrobial properties.

Keywords: 4-Acyl pyrazolone, Phenylhydrazone, Schiff base, Transition metal complex, DFT study, Antimicrobial activity

Pyrazolone and its acyl derivatives have great importance in coordination chemistry due to several electron-rich donor sites and their applications in several fields[1-7]. Acyl pyrazolone and its derivatives are widely recognized for their versatile applications in various fields, including DNA binding[8,9], dyes and pigments[10],kinetic studies[11,12], catalysts[13,14], and the pharmaceutical industry[15-18].Furthermore, in the field of analytical chemistry, acyl Pyrazolone is widely employed for the determination and extraction of various ions owing to its exceptional extracting capacity, intense colour exhibited by the complex extracts, and limited solubility of the complex in certain solvents. Notably, acyl pyrazolone and their ligand is recognized for its propensity towards keto-enol tautomerism when in a solution state[19,20].

The progress and development of coordination chemistry since several decades changed the face of modern chemistry and has made excellent contributions for the advancement of chemical and pharmaceutical industries, to design and develop organic compounds, energy sector, scientific research, catalysis and many other areas[21]. The main progress is the basic understanding of structures of compounds, several properties of complexes, and highly reactive intermediate species has changed the entire scenario in the field of metal-containing compounds. Nowadays the use of transition metal complexes has brought transformation in this field by the use of metal-containing compounds in nanoparticles, synthesis and reagents[19,22,23].

In recent years, DFT has emerged as a preferred computational method for accurately predicting the electronic structure of molecular systems. Its popularity stems from its notable accuracy in replicating experimental values of geometry, dipole moment, and various electronic properties[24]. Also, it shows potent activity as an antibiotic, antiviral, antifungal, anticancer, analgesic, and antimalarial agents[25-28]. Many complexes with different transition metals, and ligands have been prepared and studied as potent agents against the virus[29-31].

Transition metal complexes, particularly those formed with hydrazone ligands, have shown

significant antimicrobial effectiveness against both gram-positive and gram-negative bacteria[32,33]. In the present work, we have synthesized Cr(III) complexes with 4-acyl pyrazolone and evaluated their antibacterial activity. The results demonstrate that these complexes exhibit good antibacterial properties. This research not only advances the development of new drugs but also provides insights into the coordination chemistry of transition metals with heterocyclic ligands.

Experimental Section

Materials

The chemicals, l-phenyl-3-methyl-5-pyrazolone and $CrCl_3 \cdot 6H_2O$, were acquired from Sigma Ltd (India). Additionally, the acyl chlorides were purchased from Spectrochem in Mumbai, India.

Method

Fourier Transform Infrared (FT-IR) Spectroscopy: FT-IR spectra were acquired using KBr pellets on a Shimadzu 8201 PC spectrometer. Proton Nuclear Magnetic Resonance (1H NMR) Spectroscopy: 1H NMR spectra were recorded on a Bruker Advance 400 FT-NMR instrument, utilizing DMSO-d6 as the solvent. Fast Atom Bombardment Mass (FAB-MS) Spectrometry: The FAB-mass spectrum of the complex was obtained using a JEOL SX-102/2500 Da mass spectrometer with a resolution of 10,000. Thermogravimetric Analysis (TGA) and Differential Scanning Calorimetry (DSC): Simultaneous TGA/DTG and DSC analyses were performed on a PERKIN ELMER Model Diamond TG/DTA instrument. The experiment was conducted at a heating rate of 10°C per minute under a N_2 atmosphere. The chromium metal content was determined through a gravimetric method as Cr_2O_3.

General procedure for pyrazolone-based phenylhydrazone ligands (L1 to L5)

A solution of 4-sulphonamide phenylhydrazine (3.73 g, 20 mmol) in methanol (25 ml) was added dropwise to a separate solution of 1-phenyl-3-methyl-4-acetyl-5-pyrazolone (4.32 g, 20 mmol), 1-phenyl-3-methyl-4-propionyl-5-pyrazolone (4.60 g, 20 mmol), 1-phenyl-3-methyl-4-butyryl-5-pyrazolone (4.88 g, 20 mmol), 1-phenyl-3-methyl-4-benzoyl-5-pyrazolone (5.56 g, 20 mmol), and 1-phenyl-3-methyl-4-nitrobenzoyl-5-pyrazolone (6.46 g, 20 mmol) dissolved in methanol (25 ml). The addition process was carried out over a period of 20-30 minutes. Next, a small quantity of acetic acid was introduced as a catalyst, and the resulting mixture was refluxed at 60 ºC with continuous stirring for a duration of 4 hours. Throughout the reaction, the progress of the chemical transformation was monitored using thin-layer chromatography (TLC) analysis. Upon completion of the reaction, the mixture was allowed to cool to room temperature overnight, facilitating the formation of a solid product. The solid product was subsequently separated by filtration and subjected to thorough washing with diethyl ether. Following the washing step, the product was dried, and a recrystallization process was performed using R-spirit as the solvent.[34] The structure of all the ligands were confirmed by IR, 1H NMR, 13C NMR, and mass spectroscopy.

Acylated Pyrazolone (L_1): Mol. Formula $C_{18}H_{19}N_5O_3S$; m.p.218°C, Yield: 78%, Light Pink; FT-IR (KBr, cm^{-1}); 1543 ν(C=N), 3240 ν(N-H), 3340 ν(O-H), 1625 ν(C=O); 1H NMR (400 MHz, DMSO-d6): 2.48-2.49 (3H, s, $–CH_3$); 2.3 (3H, s, $–CH_3$); 6.86-7.98 (Ar-H). ^{13}C NMR (DMSO-d6) δ (ppm): 14.6 ($–CH_3$), 14.34 ($–CH_3$), 98.35-165.34 (Ar-C). M/Z= 386.3. Elemental analysis (Cal.) C: 56.09%, H: 4.97%, N: 18.17%. Found, C: 56.12%, H: 4.99%, N: 18.09%.

Propiyonal Pyrazolone (L_2): Mol. Formula $C_{19}H_{21}N_5O_3S$; m.p.215°C, Yield: 76%, Cream Powder; FT-IR (KBr, cm^{-1}); 1539 ν(C=N), 3251 ν(N-H), 3348 ν(O-H), 1600 ν(C=O); 1H NMR (400 MHz, DMSO-d6): 1.20-2.24 (3H, t, $–CH_3$); 2.5 (3H, s, $–CH_3$); 6.89-7.99 (Ar-H). ^{13}C NMR (DMSO-d6) δ (ppm): 13.31 ($–CH_3$), 16.89 ($–CH_3$), 97.26-165.91 (Ar-C). M/Z= 400. Elemental analysis (Cal.) C: 57.13%, H: 5.30%, N: 17.55%. Found, C: 57.15%, H: 5.32%, N: 17.55%.

Butyryl Pyrazolone (L_3): Mol. Formula $C_{20}H_{23}N_5O_3S$; m.p.218°C, Yield: 76%, White; FT-IR (KBr, cm^{-1}); 1531 ν(C=N), 3226 ν(N-H), 3358 ν(O-H), 1618 ν(C=O); 1H NMR (400 MHz, DMSO-d6): 2.5 (3H, s, $–CH_3$); 0.97-1.60 (3H, t, $–CH_3$); 1.60-1.64 (2H, q, $–CH_2$); 2.71-2.75 (2H, m, $–CH_2$); 6.86-7.99 (Ar-H). ^{13}C NMR (DMSO-d6) δ (ppm): 14.6 ($–CH_3$), 14.34 ($–CH_3$), 98.35-165.34 (Ar-C). M/Z= 414. Elemental analysis (Cal.) C: 58.09%, H: 5.61%, N: 16.94%. Found, C: 58.12%, H: 5.64%, N: 16.96%.

Benzoyal Pyrazolone (L_4): M.F. $C_{23}H_{21}N_5O_3S$; m.p.256°C, Yield: 71%, Light Pink; FT-IR (KBr, cm^{-1}); 1516 ν(C=N), 3182 ν(N-H), 3342 ν(O-H), 1695

ν(C=O); 1H NMR (400 MHz, DMSO-d6): 1.88 (3H, s, –CH_3); 6.86-7.98 (Ar-H). M/Z= 448. Elemental analysis (Cal.) C: 61.73%, H: 4.73%, N: 15.65%. Found, C: 61.75%, H: 4.71%, N: 15.67%.

4-Nitrobenzoyl Pyrazolone (L_5): Mol. Formula $C_{23}H_{20}N_6O_5S$; m.p.216°C, Yield: 62%, Yellow; FT-IR (KBr, cm^{-1}); 1558 ν(C=N), 3076 ν(N-H), 3200 ν(O-H), 1597 ν(C=O); 1H NMR (400 MHz, DMSO-d6): 1.92 (3H, s, –CH_3); 7.14-8.24 (Ar-H). M/Z= 493. Elemental analysis (Cal.) C: 56.09%, H: 4.09%, N: 17.06%. Found, C: 56.11%, H: 4.12%, N: 17.09%.

General procedure for complex synthesis

Cr(III) complexes afforded by the reaction of L_1-L_5 ligands with the chromium salt $CrCl_3{\cdot}6H_2O$ in 2:1(L, M) molar ratio. A methanolic solution (20 ml) of a transition metal salt $CrCl_3{\cdot}6H_2O$ (10 mmol) was taken in a round bottom flask and stirred it for few minutes. The solution became a homogeneous green. After that, a methanolic solution (30 ml) of ligands L_1-L_5 (20 mmol) was added gradually in the above solution; *p*H was maintained at 7 to 7.5 by adding alcoholic ammonia solution and allowing the mixture to stir over 4-5 hours at refluxed temperature. Solid coloured product was formed during the reaction. Isolate the product by vacuum filtration. Washed the product by distilled water, and methanol and dried it in a vacuum desiccator over $CaCl_2$.

Computational Study

Chromium (III) metal complexes $[Cr(L_1)_2Cl.H2O]$ $[ML_1]$ were synthesized and characterized, confirming distorted octahedral geometry. No prior research has thoroughly explored their experimental structures or electronic properties. This DFT study includes geometry optimization, FMO and electronic parameters, MEP analysis, Mulliken Charge, and Hirshfeld surface area analysis for both ligands and metal complexes. Calculations were performed using GAUSSIAN 09 rev software package[35] and visualized with GAUSSVIEW 6.0[36]. The study provides detailed insights into the electronic and structural characteristics of these complexes.

Calculation Parameter

Calculations were performed using GAUSSIAN 09 with the B3LYP functional which combines Becke's three-parameter hybrid exchange functional with the Lee-Yang-Parr correlation functions, and 6-31G(d, p) basis set, including polarization functions for hydrogen atoms to determine the ground state geometries of ligands and metal complexes. For metal atoms in the gas phase, the DFT/B3LYP functional with the 6-31G(d, p) basis set was used. This comprehensive approach ensured the optimization of molecular geometries and bond parameters. Additionally, calculations for FMO, Mulliken Charges, MEP, 2D fingerprint plots, and Hirshfeld surface area analysis were conducted using the same basis set.

Results and Discussion

The general procedure for the synthesis of ligands is mentioned in the experimental section and the structure of synthesized ligands (L_1-L_5) is shown in Fig. 1.

^{1}H NMR analysis (L_1-L_5)

Pyrazolone and 4-acyl Pyrazolone is known for keto-enol tautomerism and it is found in many studies. The 1H NMR data of synthesized ligands were carried out in DMSO-d6 solvent at room temperature. All the obtained data is represented in the experimental section, in the case of ^{1}H NMR spectra of the ligand peak obtained near to 12 ppm correspond to the –OH group. Aromatic protons in L_1 to L_5 ligands are observed in the range of 6.8-8.2 δ ppm. Singlet of methyl group is observed in the range 1.5 to 3.0 δ ppm in L_1 to L_5. All the data supports the structure of synthesized ligands. Based on this data it is also observed that ligands exist in keto-enol form in the solution state.

The general procedure for the synthesis of the complex is mentioned in the experimental section and the proposed structure of the Cr(III) complex is

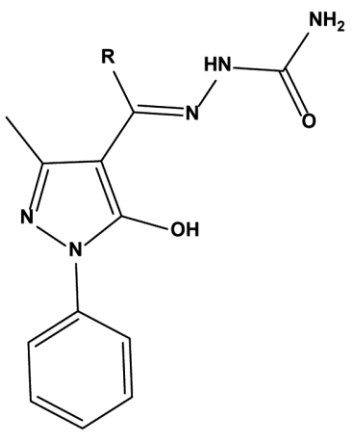

Sr. No.	Ligand	R
1.	L_1	-CH_3
2.	L_2	-C_2H_5
3.	L_3	-C_3H_7
4.	L_4	-C_6H_5
5.	L_5	-$C_6H_5NO_2$

Fig. 1 — Structure of the Schiff base ligand

expressed in Fig. 2. The synthesized Cr(III) complexes are in the solid state. They are not soluble in common organic solvents, solubility of these complexes is in the solvents like DMF and DMSO. Physico-analytical data of complexes are indicated in Table 1.

Infrared Spectra

The infrared (IR) spectra of ligands (L_1-L_5) and their Cr(III) metal complexes provide detailed information about the nature of functional groups attached to the metal ion. In the IR spectra of ligands (L1-L5), a sharp peak is observed in the 1531-1560 cm^{-1} range, corresponding to the acyclic azomethine group. In the complexes, where the ligands coordinate to the metal through the nitrogen atom, a reduction in electron density in the azomethine link is expected, resulting in the appearance of a peak in the 1512-1535 cm^{-1} range[37]. The IR spectrum of the ligands exhibits a prominent band in the 1595-1625 cm^{-1} range, attributed to the stretching mode of the υ(C=O) group. Upon complexation, this band disappears, and a new band emerges in the 1566-1597 cm^{-1} range, suggesting the involvement of oxygen in the complex formation. Furthermore, the proposed coordination sites are supported by medium bands observed between 408-447 cm^{-1} and 493-563 cm^{-1}, which can be attributed to the ν(M-N) and ν(M-O) modes, respectively[38,39].

Based on the above discussion, it can be concluded that the coupling process between the ligands and the metal ion leads to the formation of complexes.

Electronic Spectral Studies

The electronic spectral data shown in Fig. 3 provided information on the geometry of the Cr(III) complexes based on phenyl hydrazone ligands. The electronic spectra of the free ligands (L_1-L_5) displayed a strong band in the range of 32467-30395 cm^{-1} (Fig. 4). This intense band can be attributed to intra-ligand charge transition (ILCT). In the electronic

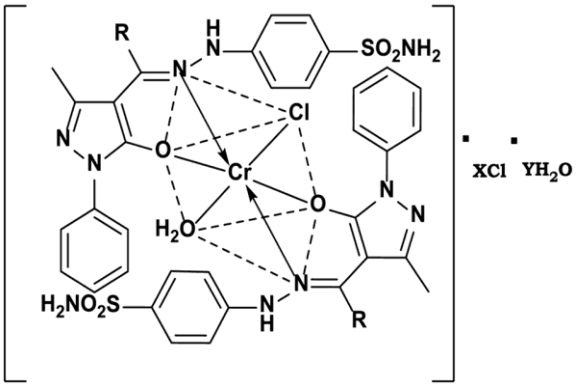

Fig. 2 — Proposed structure of Cr(III) Complexes

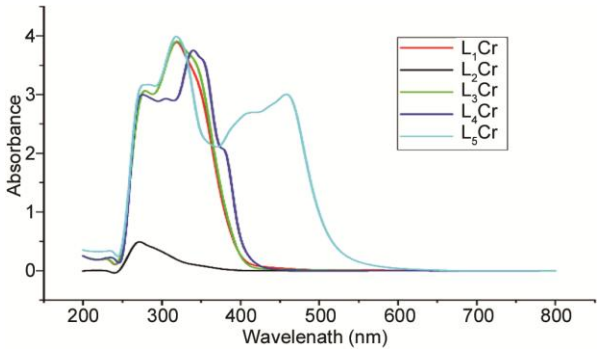

Fig. 3 — UV spectra of L_1Cr to L_5Cr

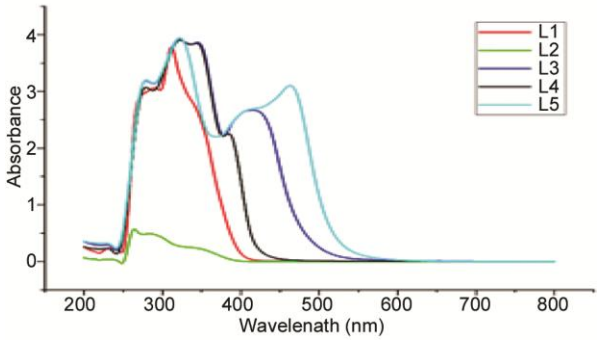

Fig. 4 — UV spectra of L_1 to L_5

Table 1 — Physico-Analytical Data of Complex

Sr. no.	Complex	Formula Weight	Colour (%Yield)	C	H	N	O	S	Cl	Cr
1	$[Cr(L_1)_2Cl{\cdot}H_2O]{\cdot}Cl{\cdot}H_2O$	927	Brown (74)	46.62 (46.60)	4.32 (4.35)	15.08 (15.10)	13.78 (13.80)	6.93 (6.91)	7.66 (7.64)	5.61 (5.60)
2	$[Cr(L_2)_2Cl{\cdot}H_2O]{\cdot}2H_2O$	920	green (65)	49.62 (49.59)	4.84 (4.82)	15.23 (15.22)	13.90 (13.91)	6.99 (6.97)	3.83 (3.85)	5.62 (5.65)
3	$[Cr(L_3)_2Cl{\cdot}H_2O]{\cdot}H_2O$	930	brown (69)	53.67 (51.64)	4.97 (4.98)	15.07 (15.05)	12.06 (12.04)	6.91 (6.89)	3.83 (3.81)	5.61 (5.59)
4	$[Cr(L_4)_2Cl{\cdot}H_2O]{\cdot}Cl{\cdot}1.5H_2O$	1033	Brown (71)	53.43 (53.44)	4.11 (4.09)	13.53 (13.55)	10.84 (10.83)	6.22 (6.20)	6.89 (6.86)	5.05 (5.03)
5	$[Cr(L_5)_2Cl{\cdot}H_2O]{\cdot}2Cl{\cdot}2H_2O$	1088	green (63)	50.77 (50.76)	3.72 (3.70)	15.41 (15.44)	16.15 (16.17)	5.91 (5.89)	3.28 (3.26)	4.79 (4.78)

spectra of the complexes, two bands were observed at approximately 20,000 and 32,500 cm^{-1}, which were assigned as MLCT (metal-to-ligand charge transfer) transitions. The calculated magnetic moment of these Cr(III) complexes was found to be 3.87 B.M. In the present study, the electronic spectra of the Cr(III) complexes revealed charge transfer bands and d-d transitions. The bands observed in the range of 21691-18939 cm^{-1} in the complexes were associated with d-d transitions. The calculated magnetic moment of these Cr(III) complexes was 3.87 B.M. Based on the investigations, all the studied complexes were found to be six-coordinated, indicating distorted octahedral geometry for the complexes.

Mass Spectral Study (FAB)

The mass spectral study of metal complex $[Cr(L_1)_2Cl{\cdot}H_2O]{\cdot}Cl{\cdot}H_2O$ has been carried out and shown in Fig. 5. The mass spectra of the metal complex indicate that the molecular ion peak at m/z=928 coincident with the formula weight of the metal complex. Also, the sharp peak observed at m/z=820 represents the base peak with 99% abundance. The suggested fragmentation pattern is indicated in Scheme 1.

Thermal Studies

The thermal stability of the metal complexes was evaluated using thermogravimetric analysis (TGA-DTG) under a nitrogen atmosphere, with a temperature range of 50-1000°C. Additionally, differential scanning calorimetry (DSC) studies were conducted within the temperature range of 50-600°C. The relationship between the different stages of decomposition of the metal complexes and their corresponding weight losses were determined based on the proposed structures of the complexes.

The TGA-DTG analysis of the complex $[Cr(L_1)_2Cl{\cdot}H_2O]{\cdot}Cl{\cdot}H_2O$ is presented in Fig. 6. The decomposition of this complex occurs in multiple steps. The first step, observed between 50-210°C, results in a mass loss of 6.08% (6.05%). This stage involves the loss of one crystalline Cl and H_2O. The second step, occurring in the temperature range of 211-300°C, corresponds to the decomposition of one coordinated H_2O and one coordinated Cl, resulting in a mass loss of 15.56% (15.53%). The third stage involves the decomposition of the residual part of the L1 ligand and an estimated amount of Cr oxide, taking place in the temperature range of 301-950°C, with a mass loss of 47.09% (47.08%). Overall, the observed mass loss is 68.66%, compared to the theoretical value of 68.73%. Each of these stages is accompanied by an endothermic effect at 66.1°C, 186.4°C, 235°C, and 282.9°C, as shown in the DSC curve (Fig. 7). A summary of the assignments for all the complexes is presented in Table 2.

Computational Measurement

Geometry Optimization

The geometry optimization of ligands L_1 and their chromium (III) complexes $[Cr(L_1)_2Cl.H2O]$ $[ML_1]$, was performed in the vacuum phase. Bond lengths and angles, shown in Fig. 8 and Table 3, confirm the distorted octahedral geometry of the Cr(III) complexes. Vibrational frequency calculations revealed no

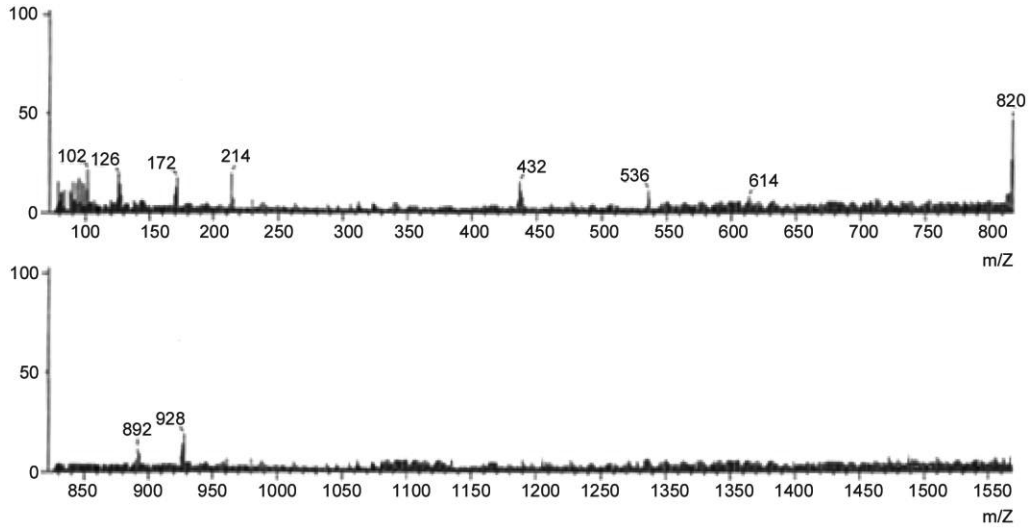

Fig. 5 — FAB mass spectrum of $[Cr(L_1)_2Cl{\cdot}H_2O]{\cdot}Cl{\cdot}H_2O$

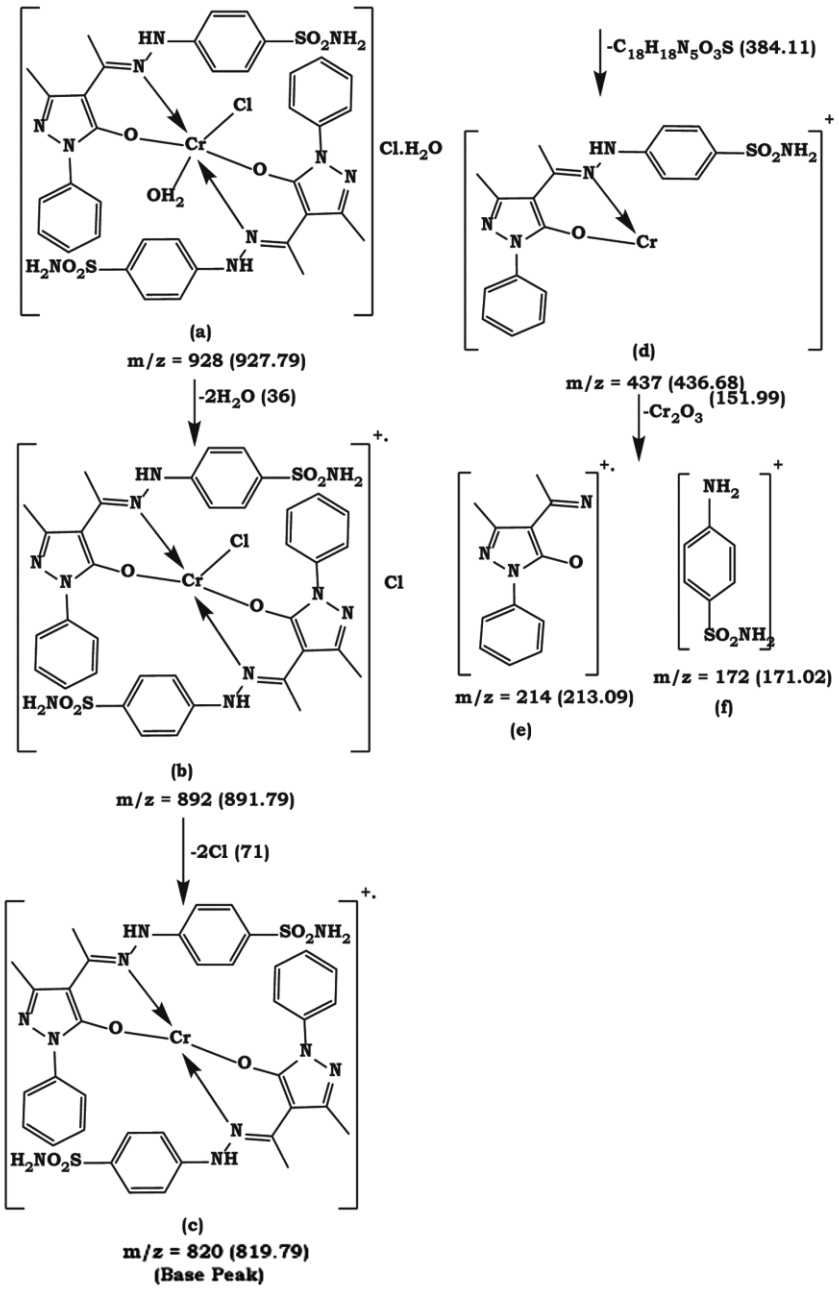

Scheme 1 — Suggested fragmentation pattern of $[Cr(L_1)_2Cl{\cdot}H_2O]{\cdot}Cl{\cdot}H_2O$

imaginary frequencies, indicating successful optimization. The optimized structures are detailed in Fig. 8.

FMO – Frontier Molecular Orbitals and Reactivity Parameters

HOMO and LUMO, the Frontier Molecular Orbitals (FMOs), are crucial for understanding molecular interactions and electronic properties. Their energy levels indicate various electronic properties like chemical stability and reactivity. The energy gap between HOMO and LUMO reveals details such as ionization potential, chemical potential, and electron affinity. Fig. 9 displays the energy diagrams of HOMO and LUMO for ligands and their Cr(III) complexes. Negative values of E_{HOMO} and E_{LUMO}, along with negative chemical potential, highlight the stability of the ligands and complexes.

Energy gap (ΔE)	$=E_{LUMO} - E_{HOMO}$	1
Ionization potential (IP)	$=- E_{HOMO}$	2
Chemical potential (μ)	$=½ (E_{HOMO} + E_{LUMO})$	3

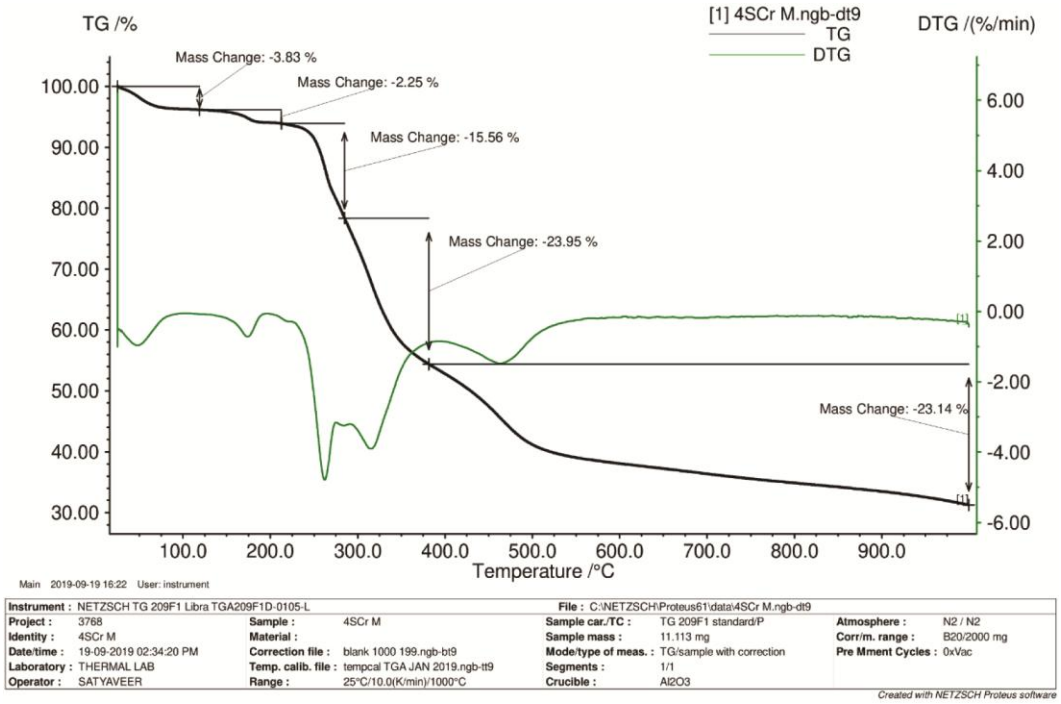

Fig. 6 —TGA/DTG curve of $[Cr(L_1)_2Cl{\cdot}H_2O]{\cdot}Cl{\cdot}H_2O$

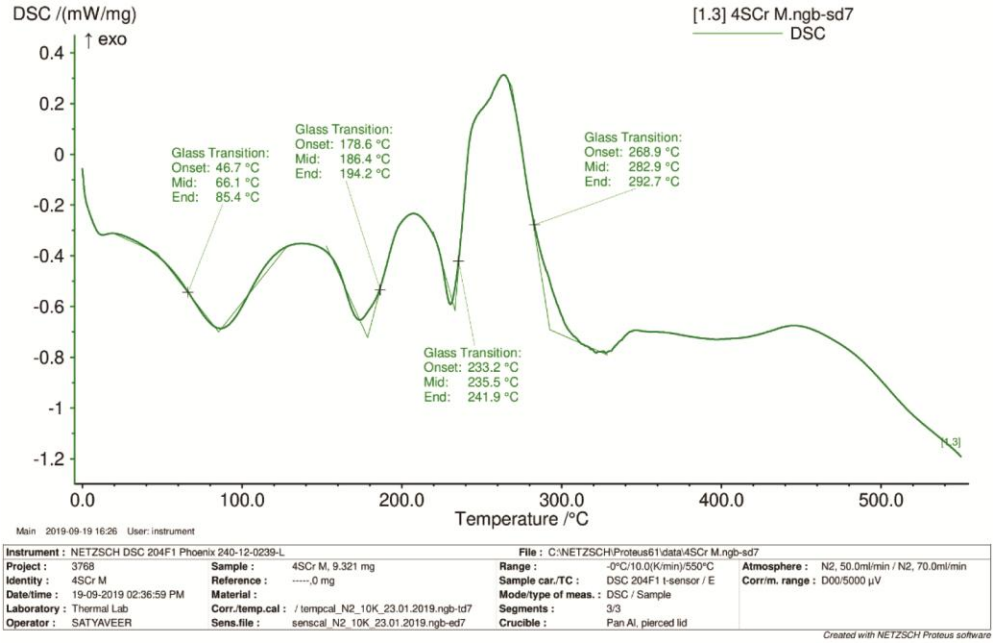

Fig. 7 — DSC curve of $[Cr(L_1)_2Cl{\cdot}H_2O]{\cdot}Cl{\cdot}H_2O$

Electron affinity (EA)	$=-E_{LUMO}$	4
Electron Negativity (EN)	$=-½\,(E_{HOMO}+E_{LUMO})$	5
Global Hardness (ɳ)	$=-½\,(E_{HOMO}-E_{LUMO})$	6
Softness (S)	$=1/2ɳ$	7
Electrophilicity Index (ω)	$=\mu^2/2ɳ$	8

Table 4 shows the electronic parameters of Ligand and Complex.

Molecular Electrostatic Potential (MEP)

MEP surfaces were generated to predict reactive sites for ligands and their Cr(III) complex. These surfaces illustrate charge distribution, with red for electrophilic (negative charge), blue for nucleophilic (positive charge), and green for neutral regions. MEP maps aid in understanding stability and reactivity

Table 2 — Thermo analytical results of Complex

Complexes	Temp. Range	Mass Loss (%) Obs. (Cal.)	Analysis
$[Cr(L_1)_2Cl{\cdot}H_2O]{\cdot}Cl{\cdot}H_2O$	50-210	6.08(6.05)	Crystalline Cl and H_2O may loss.
	211-300	15.56(15.53)	Coordinated H_2O and Cl may loss.
	301-950	47.09(47.08)	Portion of the ligand may be lost, leaving behind the oxide of chromium (Cr).
$[Cr(L_2)_2Cl{\cdot}H_2O]{\cdot}2H_2O$	50-220	3.89(3.91)	Two crystalline H_2O may loss
	221-345	7.77(7.81)	Coordinated H_2O and Cl may loss.
	346-950	53.37(53.40)	Portion of the ligand may be lost, leaving behind the oxide of chromium (Cr).
$[Cr(L_3)_2Cl{\cdot}H_2O]{\cdot}H_2O$	50-345	9.65(9.66)	One crystalline H_2O may loss
	346-556	26.46(26.50)	Coordinated H_2O and Cl may loss.
	557-950	32.69(32.70)	Portion of the ligand may be lost, leaving behind the oxide of chromium (Cr).
$[Cr(L_4)_2Cl{\cdot}H_2O]{\cdot}Cl{\cdot}1.5H_2O$	50-235	5.86(5.87)	One crystalline Cl and $1.5H_2O$ may loss.
	236-443	7.97(7.98)	Coordinated H_2O and Cl may loss.
	444-950	49.68(49.7)	Portion of the ligand may be lost, leaving behind the oxide of chromium (Cr).
$[Cr(L_5)_2Cl{\cdot}H_2O]{\cdot}2Cl{\cdot}2H_2O$	50-243	8.91(8.93)	Two crystalline Cl and two H_2O may loss.
	244-451	9.41(9.42)	Coordinated H_2O and Cl may loss.
	452-950	52.68(52.7)	Portion of the ligand may be lost, leaving behind the oxide of chromium (Cr).

Table 3 — Bond angle Ligand [L1] and Chromium (III) Complex

Sr. No	L1		ML1	
	Atom With Label	Bond Angle (˚)	Atom With Label	Bond Angle (˚)
1.	C1 - O6 - H28	113.5923	O14 – Cr55 – N16	98.37
2.	C2 - C14 - N16	124.4669	N16 – Cr55 – Cl56	75.43
3.	C14 - N16 - N17	109.0059	Cl56 – Cr55 – O33	92.83
4.	N16 - N17 - C18	107.5929	O33 – Cr55 – N36	89.40
5.	N16 - N17 - H40	117.2641	N36 – Cr55 – O57	70.76
6.	C18 - N17 - H40	106.3162	O57 – Cr55 – O14	92.83

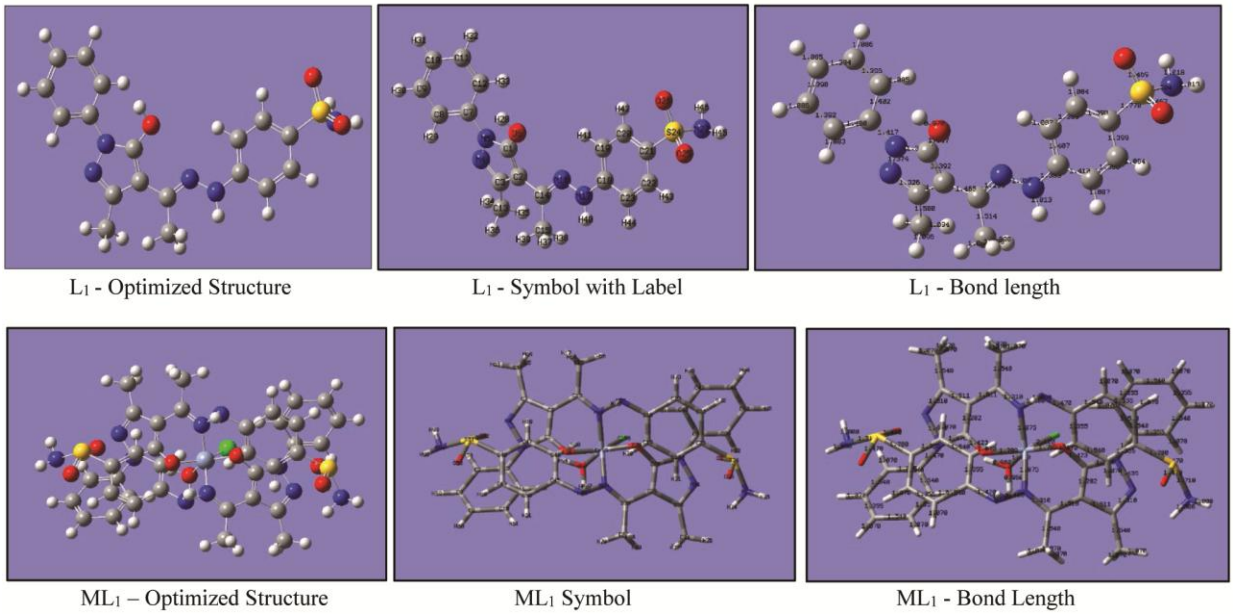

Fig. 8 —Optimized Structure of Ligand L1 and ML1

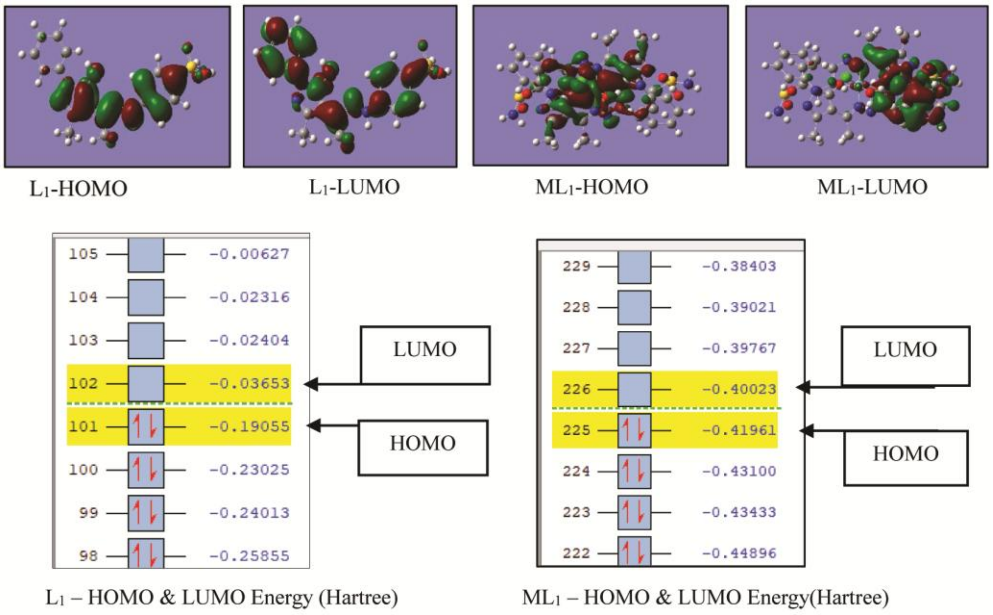

Fig. 9 — Ligand L_1& ML_1: HOMO – LUMO and Energy Diagram

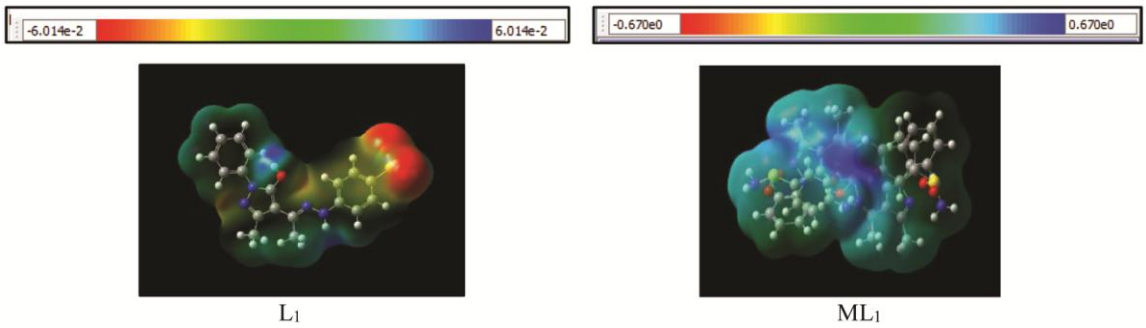

Fig. 10 — MEP Surface – Ligand L_1 and Complex ML_1

Table 4 — Electronic Properties of Ligand and Cr(III) complex

Sr. No.	Properties	L1	ML1
1.	Total Energy (K eV)	–43.39	–129.70
2.	E_{HOMO} (eV)	–5.1851	–11.4181
3.	E_{LUMO} (eV)	–0.9940	–10.8908
4.	ΔE (eV)	4.19110	0.5273
5.	Ionization potential (IP) (eV)	5.1851	11.4181
6.	Chemical potential (μ) (eV)	–3.0895	–11.1544
7.	Electron affinity (EA) (eV)	0.9940	10.8908
8.	Electron Negativity (EN) (eV)	3.0895	11.1544
9.	Global Hardness (ɳ) (eV)	2.0955	0.2673
10.	Softness (S) (eV^{-1})	0.2386	1.8705
11.	Electrophilicity Index (ω) (eV)	2.2775	232.7359
12.	Dipole Moment (Debye)	5.868544	2.756491

towards nucleophiles and electrophiles. Typically, the MEP colour spectrum ranges from red (lowest potential) to blue (highest potential), with red, orange, and yellow indicating electron-donating areas, while green and blue indicate electron-accepting areas[40]. Fig. 10 shows the electrostatics surface of Ligand and their complex.

Mulliken Charge

The Mulliken charge of the ligand and the Cr(III) complex was determined through calculations utilizing the B3LYP/6-31G(d,p) method. These calculations are crucial in quantum mechanical computations applied to molecular systems[41]. The distribution of charges within compounds influences polarizability, dipole moment, and electronic structure[42]. Fig. 11 displays the computed Mulliken charge of ligand and metal complexes.

2D fingerprint with Hirshfeld surface area analysis

Hirshfeld surface area analysis, developed by Ronald G. Hirshfeld, predicts intermolecular interactions and molecular surface properties using electron density distribution. This method, often using

DFT calculations, generates 2D fingerprints and surface parameters like d_{norm}, d_i, d_e, shape index, curvedness, and fragment patch through Crystal Explorer 17 software. Colour-coded Hirshfeld surfaces highlight interactions: red patches indicate strong hydrogen bonding (short contacts), while blue patches signify weaker or absent interactions (long contacts). For ligands and their Cr(III) complexes, minimal Cr interactions suggest no significant neighbouring atom interactions. Fig. 12-14 illustrate 2D fingerprint plots, providing insights into the structural characteristics and molecular interactions of these compounds. Overall, Hirshfeld surface analysis is crucial for understanding molecular recognition and stability[43-45].

In vitro antimicrobial study

The antimicrobial efficacy of ligands L_1 to L_5 and their corresponding Cr(III) complexes was assessed through *in vitro* experiments utilizing the agar well diffusion method. The selected microorganisms for screening included gram-positive strains such as *Bacillus megaterium, Staphylococcus aureus,* and *Bacillus subtilis*, as well as gram-negative strains encompassing *E. coli* and *Klebsiella*. Overall, the tested compounds demonstrated significant antimicrobial activity against gram-positive bacteria in comparison to gram-negative bacteria (Fig. 15 and Table 5).

Notably, certain complexes exhibited superior bactericidal potency when compared to the

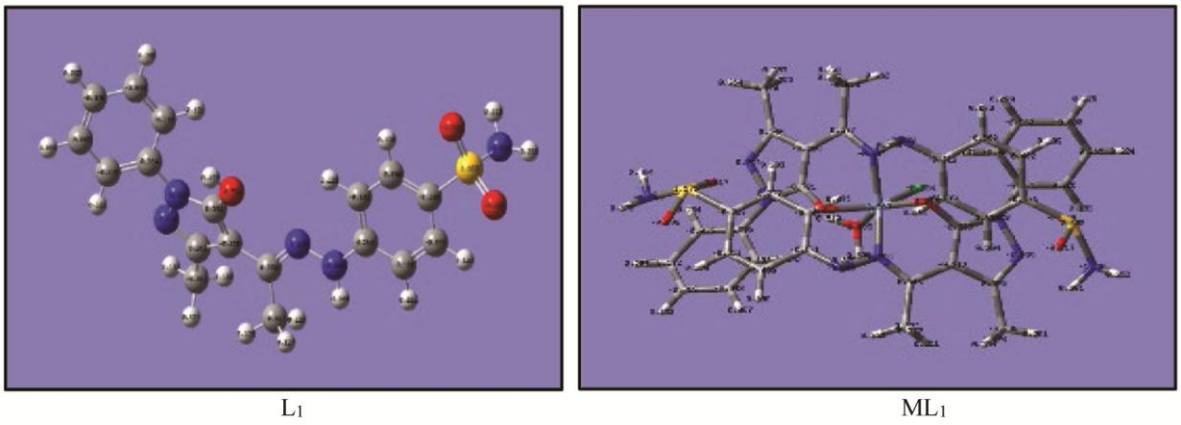

Fig. 11 — Mulliken Charges of Ligand L1 & Metal Complex ML_1

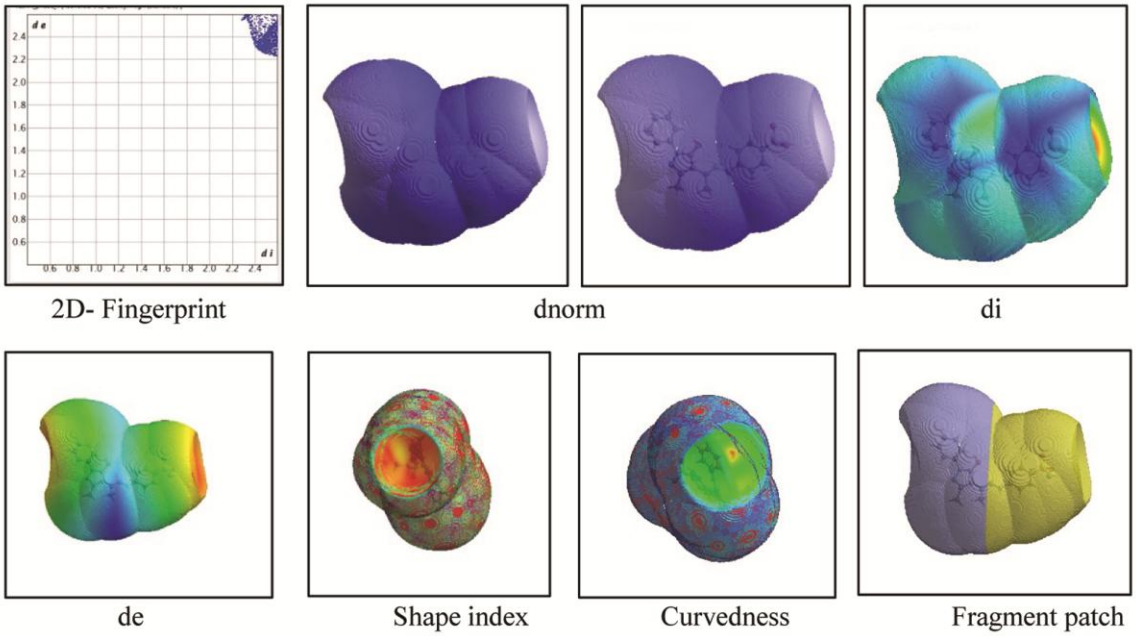

Fig. 12 — The Molecular Hirshfeld (2D Fingerprint, dnorms , di, de, Curvedness, Fragment Patch) Ligand L1

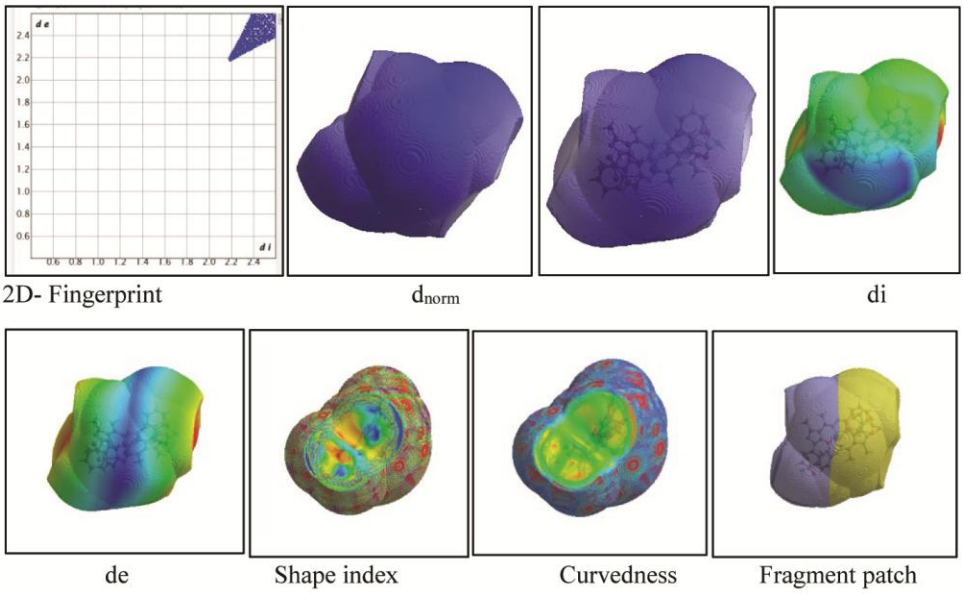

Fig. 13 — The Molecular Hirshfeld (2D Fingerprint, dnorms , di, de, Curvedness, Fragment Patch) Complex ML1

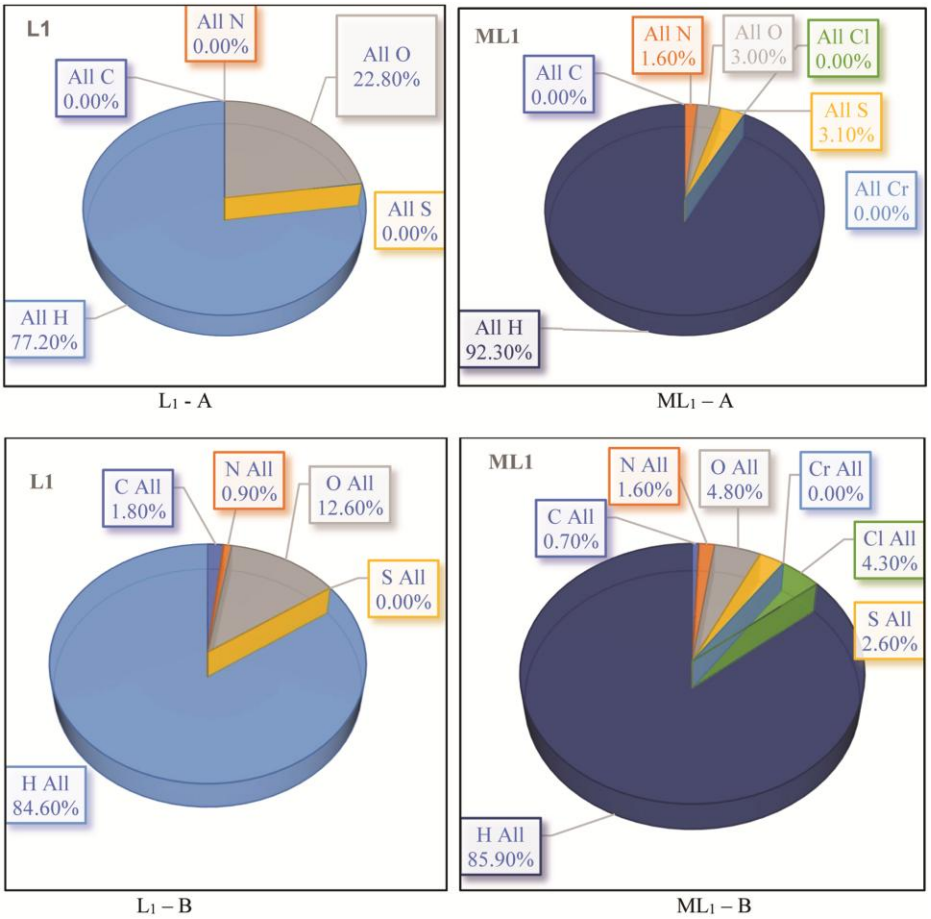

Fig. 14 — (A) Inside atom to outside atom interaction in L_1 ligand and ML_1 complex;(B) Inside atom to other atoms interaction in L_1 ligand and ML_1 complex

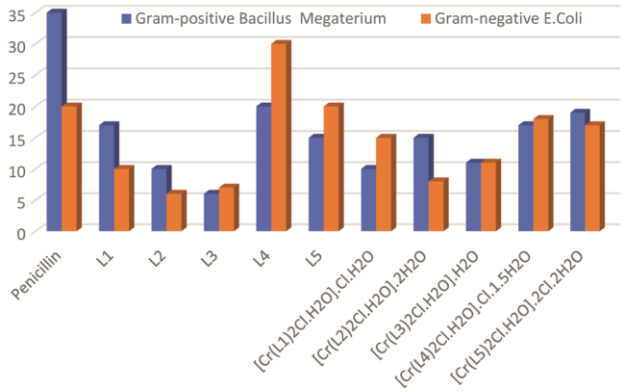

Fig. 15 — Antimicrobial Effects of the Ligands and their Cr(III) Complexes, Zone of Inhibition (mm)

Table 5 — Antimicrobial Effects of the Ligands (L_1-L_5) and their Cr(III) Complexes, Zone of Inhibition (mm)

Sr. No.	Compd	Gram-positive *Bacillus megaterium*	Gram-negative *E. coli*
Ref. Drug	Penicillin	35	20
1	L_1	17	10
2	L_2	10	06
3	L_3	06	07
4	L_4	20	30
5	L_5	15	20
6	$[Cr(L_1)_2Cl{\cdot}H_2O]{\cdot}Cl{\cdot}H_2O$	10	15
7	$[Cr(L_2)_2Cl{\cdot}H_2O]{\cdot}2H_2O$	15	08
8	$[Cr(L_3)_2Cl{\cdot}H_2O]{\cdot}H_2O$	11	11
9	$[Cr(L_4)_2Cl{\cdot}H_2O]{\cdot}Cl{\cdot}1.5H_2O$	17	18
10	$[Cr(L_5)_2Cl{\cdot}H_2O]{\cdot}2Cl{\cdot}2H_2O$	19	17

corresponding ligands. The enhanced antimicrobial activity of the complexes can be attributed to the principles outlined in Overtone's concept[46] and Tweedy's chelation theory[47]. Overtone's concept underscores the significance of compound solubility in determining its antimicrobial effectiveness. Upon complex formation, metal ions undergo a reduction in polarity. Additionally, the complexes exhibit increased π-electron delocalization, thereby enhancing their lipophilicity and facilitating easier penetration into microbial cells, ultimately exerting control over their growth[48]. The remarkable antimicrobial activities observed in these compounds against the tested organisms strongly warrant further investigations.

Conclusion

In conclusion, the synthesis and structural analysis of Pyrazolone-based Phenylhydrazone ligands were successfully carried out using spectroscopic techniques. The results indicated that these ligands predominantly exist in the enol form, with the presence of intramolecular hydrogen bonding. To explore their potential applications, a series of complexes based on Cr(III) transition metals were synthesized and characterized using various analytical techniques. The characterization process involved FT-IR, UV, FAB mass spectrometry, TGA, DTG, DSC, and elemental analysis. The comprehensive theoretical study presented provided valuable insights into the structural and electronic properties of pyrazolone ligands and their Chromium(III) complexes. The results obtained from geometry optimization, FMO analysis, MEP mapping, Mulliken charge distribution, 2D fingerprint and Hirshfeld surface analysis contribute to a thorough understanding of the studied systems, laying the groundwork for further exploration of their potential application in various fields. Remarkably, the biological evaluation of these complexes revealed their significant activity against both Gram-positive and Gram-negative organisms, surpassing the activity of the corresponding ligands. These findings introduce a novel class of bactericidal agents based on metal complexes, highlighting their potential as promising antimicrobial agents for further investigations and applications.

Supplementary Information

Supplementary information is available in the website http://nopr.niscpr.res.in/handle/123456789/58776.

References

1 Wang J, Xu G-C, Zhang Y-P, Luo H-Y, Li J-Y, Zhang L & Jia D-Z, *New J Chem*, 43 (2019) 2529.
2 Modi C K, & Jani D H, *App Organomet Chem*, 25 (2011) 429.
3 Marchetti F, Pettinari R & Pettinari C, *Coord Chem Rev*, 303 (2015) 1.
4 Ramadan A M, Alshehri A A & Bondock S, *J Saudi Chem Soc*, 23 (2019) 1192.
5 Kanoongo N, Bohra S, Mathur R & Mathur N K, *Trans Metal Chem*, 17 (1992) 322.
6 Raman N, Johnson R S, Joseph J, Sakthivel A & Dhaveethu R J, *J Chilean Chem Soc*, 53 (2008). (https://doi.org/10.4067/S0717-97072008000300010).
7 Shaikh I, Jadeja R N, Patel R, Mevada V & Gupta V K, *J Mol Struc*, 1232 (2021) 130051.
8 Vyas K M, Jadeja R N, Patel D, Devkar R V & Gupta V K, *Polyhedron*, 80 (2014) 20.
9 Nejati K, Rezvani Z & Massoumi B, *Dyes Pigments*, 75 (2007) 653.
10 Liu L, Jia D-Z, Ji Y-L & Yu K-B, *J Photochem Photobio A: Chem*, 154 (2003) 117.
11 Peng B, Liu G, Liu L & Jia D, *Tetrahedron*, 61 (2005), 5926.

12 Gupta K C & Sutar A K, *Coord Chem Rev*, 252 (2008) 1420. (https://doi.org/10.1016/j.ccr.2007.09.005)
13 Kumar R & Mani G, *Dalton Trans*, 44 (2015) 6896.
14 Adams H, Fenton D E, Minardi G, Mura E, Pistuddi A M & Solinas C, *Inorg Chem Comm*, 3 (2000) 24.
15 Agarwal R K & Prakash B, *Trans Metal Chem*, 30 (2005) 696.
16 Shinde N G & Pimpodkar N V, *Res J Pharm Dosage Forms Tech*, 7 (2015) 74.
17 Kataeva O N, Gubaidullin A T, Litvinov I A, Lodochnikova O A, Islamov L R, Movchan A I & Chmutova G A, *J Mol Struc*, 610 (2002) 175.
18 Doğan H N, Duran A & Yemni E, *Drug Meta Drug Interac*, 15 (1999) 187.
19 Zhang J, Sun J, Geng H, Ma Q & Li C, *Arabian J Chem*, 15 (2022) 103693.
20 Somaiya C P, Patel D S & Jani D H, *J Emerg Tech Innov Res*, 6 (2019) 247.
21 Nandaniya B, Das S P & Jani D, *Curr Chem Lett*, 12 (2023) 289.
22 Du J, Yang H, Wang C & Zhan S, *App Organomet Chem*, 36 (2022) e6572.
23 Wu X, Ma P & Wang J, *Applied Organomet Chem*, 36 (2022) e6578.
24 Kumar R, Singh H, Mazumder A, Salahuddin & Yadav R K, *Topics Curr Chem*, 381 (2023) 12.
25 Xhafa S, Di Nicola C, Tombesi A, Pettinari R, Pettinari C, Scarpelli F, Crispini A, La Deda, M, Candreva A, Garufi A, D'Orazi G, Galindo A, & Marchetti F, *Journal of Medicinal Chemistry,* 67(2024).https://doi.org/10.1021/acs.jmedchem.4c01298
26 Mezgebe K & Mulugeta E, *Med Chem Res*, 33 (2024) 439.
27 Uvarova M A, Novikova M V, Eliseenkova V A, Baravikov D E, Dolgushin F M, Bekker O B, Fatushina E V, Kiskin M A, Eremenko I L & Lutsenko I A, *Russian J Coord Chem*, 49 (2023) 680.
28 Milaeva E R & Lutsenko I A, *Russian J Coord Chem*, 49 (2023) 527.
29 Karges J & Cohen S M, *Chem Bio Chem*, 22 (2021) 2600.
30 Zibaseresht R, *SSRN Elect J*, (2020). (https://doi.org/10.2139/ssrn.3738106).
31 Zha Z, Dai X, Li C, Wang X, Tian J, Feng Y, Xie J, Ma C, Nie Z, Fan P, Qian M, He X, Wu S, Zhang Y & Zheng X, *Eur J Med Chem*, 186 (2020) 111893.
32 Somaiya C P, Patel D S & Jani D H, *J Applicable Chemistry*,8 (2019) 1135.
33 Arora T, Devi J, Dubey A, Tufail A & Kumar B, *Appl Organomet Chem*, 37 (2023) e7209.
34 Somaiya C P, Patel D S & Jani D H, *Asian J Chem*, 32 (2020) 789.
35 Frisch M J, Trucks G W, Schlegel H B, Scuseria G E, Robb M A, Cheeseman J R, Scalmani G, Barone V, Mennucci B, Petersson G A, Nakatsuji H, Caricato M, Li X, Hratchian H. P, Izmaylov A. F, Bloino J, Zheng G, Sonnenberg J L, Hada M, Ehara M, Toyota K, Fukuda R, Hasegawa J, Ishida M, Nakajima T, Y. Honda, Kitao O, Nakai H, Vreven T, Montgomery J A, Peralta J. E, Ogliaro F, Bearpark M, Heyd J J, Brothers E, Kudin K N, Staroverov V N, Kobayashi R, Normand J, Raghavachari K, Rendell A, Burant J. C, Iyengar S. S, Tomasi J, Cossi M, Rega N, Millam J M, Klene M, Knox J E, Cross J B, Bakken V, Adamo C, Jaramillo J, Gomperts R, Stratmann R. E, Yazyev O, Austin A. J, Cammi R, Pomelli C, Ochterski J W, Martin R L, Morokuma K, Zakrzewski V. G, Voth G. A, Salvador P, Dannenberg J J, Dapprich S, Daniels A. D, Farkas O, Foresman J B, Ortiz J V, Cioslowski J, & Fox D J, *Gaussian 09,Revision D. 01*,(Gaussian, Inc.: Wallingford, CT, USA) 2009.
36 Gauss View 6.0.16, *Gaussian Inc*, (Wallingford, CT, USA) 2009.
37 Jaiswal A K, Rao G P, Pandey O P & Sengupta S K, *J Agricultural Food Chem*, 46 (1998) 1609.
38 Howlader M B H& Semicarcarbazoneam M S I, *Indian J Chem*, 46A (2007) 440.
39 Thankamony M & Mohanan K, *Indian J Chem*, 46A (2007) 247.
40 Mishra P C & Kumar A, *Theor Org Chem Els Sci*, (1996).
41 Gunasekaran S, Kumaresan S, Arunbalaji R, Anand G & Srinivasan S, *J Chem Sci*, 120 (2008) 315.
42 Ojha J K, Ramesh G & Reddy B V, *Asian J Chem*, 35 (2023) 1283.
43 Spackman M A & Byrom P G, *Chem Phys Lett*, 267 (1997) 215.
44 Spackman M A & McKinnon J J, *Cryst Eng Comm*, 4 (2002) 378.
45 Ramalingam A, Kansız S, Dege N & Sambandam S, *J Chem Cryst*, 51 (2021) 273.
46 Chohan Z H, Khan K M & Supuran C T, *App Organomet Chem*, 18 (2004) 305.
47 Tweedy B G, *Phytopathology*, 55 (1964) 910.
48 Pasdar H, Saghavaz H B, Foroughifar N & Davallo M, *Molecules*, 22 (2017) 2125.